An *In Vitro* Model to Assess Early Immune Markers following Co-Exposure of Epithelial Cells to Carbon Black (nano)Particles in the Presence of *S. Aureus*: Differential Induction of Cytokines.

Scott M Brown
Swansea University
Stephen J Evans
Swansea University
Michael J Burgum
Swansea University
Llinos G Harris
Swansea University
Rowena E Jenkins
Swansea University
Shareen H Doak
Swansea University
Martin J D Clift
Swansea University
Thomas S Wilkinson (t.s.wilkinson@swansea.ac.uk)
Swansea University https://orcid.org/0000-0003-0397-6079

Research

Keywords: Epithelial cells, Lung, Skin, A549, HaCaT, Carbon black (nano)particles, Cytokines, IL-8, IL-6, human β-defensin-2 (hβD-2), Staphylococcus aureus, Immunocompromised, infection, particle exposure, in vitro co-exposure models.

Posted Date: September 22nd, 2021

DOI: https://doi.org/10.21203/rs.3.rs-907832/v1

Abstract

Human exposure to carbon black (CB) is inevitable due to its widespread applications in the medical, industrial and consumer sectors. With an ageing population, it is imperative that the effects of (nano)particle exposure in individuals with compromised immunity or infection are considered. Since barrier immunity provides the first line of defence against CB and the human skin and lung pathogen, *Staphylococcus aureus*, this work focuses on studying the impact of CB exposure upon compromised immunity during infection on human skin and lung epithelial cells *in vitro*. The principal aim of the work was to develop an epithelial cell model to characterise (co-)exposure to CB and *S. aureus*. The work used two human epithelial cell lines, HaCaT (skin) and A549 (lung), ELISA technology to assess the (pro-)inflammatory response, aseptic microbiology techniques to grow *S. aureus* and a Zetasizer, EDX spectroscopy, and both scanning and transmission electron microscopy (SEM and TEM) to characterise the CB under the conditions used in the study. Physicochemical characterisation of CB confirmed its shape, dramatic polydispersity and potential to aggregate. CB significantly inhibited *S. aureus* growth, but in a biological media dependent manner. CB did not induce cytokines or antimicrobial peptides from skin and lung epithelial cells, when given alone. In contrast, *S. aureus* induced a robust interleukin (IL)-8 response in both skin and lung epithelial cells. IL-6 and human beta defensin (hβD)-2 could only be detected when cells were stimulated with *S. aureus*. However, co-exposure to CB (100μg/ml) and *S. aureus* resulted in significant inhibition of IL-8 (compared to *S. aureus* only induced levels). Furthermore, the same co-exposure induced significantly more hβD-2 (compared to *S. aureus* alone). The ability to detect pathogen responses to particle, in addition to epithelial responses to particle and pathogen is an advance on assessing cell responses under 'healthy' conditions and supports the need for developing exposure models under stressed or immunosuppressed conditions. This model will be useful for studying mechanisms of exposure in at-risk groups, including factory workers, the elderly and immunocompromised. Advanced models, that better represent human pathophysiology are essential for understanding cellular mechanisms of toxicity in the 21st Century.

Background

Carbon black (CB) is a (nano)particle with a tendency to aggregate by fusing together creating three-dimensional branched clusters and larger agglomerates through Van der Waals forces [1]. CB can be engineered to have a wide range of practical everyday uses including rubber tyre reinforcements, printer toner, rubber soles, dry batteries, conveyor belts and flammable fluids [2–4]. It has further been widely used as a surrogate of particulate matter when assessing the human health risk to air pollution [5]. The versatility of CB is supported by the production of over 11 million metric tons in 2012 and 89% of this is used in the rubber industry [6]. While, it is clear that a high proportion of the world's population will be exposed to CB, the associated public health risk is reported to be low or non-existent. The World Health Organisation considers CB a potential carcinogen [7], however, meta-analyses of large occupational health studies suggest no associated risk with lung cancer [6]. Other studies have also suggested that CB is unlikely to be directly genotoxic, or a reproductive toxicant [8]. However, recent human [9] and animal

studies [10, 11] suggest that age and the effects of immunosuppression may have been previously underestimated.

The lung and skin are two major routes for CB exposure [12]. The local cellular mechanisms of toxicity and immunity have been studied in human lung and skin cell lines, such as A549 and HaCaT respectively. For instance, A549 and HaCaT colony formation showed significant decreases in colony size, number and viability following CB exposure [13]. CB also increased cytotoxicity as measured by lactate dehydrogenase (LDH) release [14], and genotoxicity as assessed by micronuclei frequency in A549 cells [15]. However, despite comparable concentration ranges (0-400μg/ml) not all studies could detect cellular toxicity, as Horie and co-workers found no effects of CB on cell proliferation and intracellular reactive oxygen species (ROS) [16]. CB also produces a strong (pro-)inflammatory response through the release of macrophage chemotaxins from epithelial cells [17] and serum [18], as well as IL-8 production in A549 cells [14]. Indeed, it is clear that CB may also inhibit the antimicrobial functions of the antimicrobial peptide, LL-37, in A549 cells [19]. However, very little work has assessed how these responses may differ under immunosuppressed conditions or during skin and lung infection.

Staphylococcus aureus is as a major pathogen in the skin and lungs, causing significant disease burden to health services worldwide [20]. *S. aureus* is an opportunistic pathogen in those individuals that are immunosuppressed and immunocompromised [21]. In the lungs, *S. aureus* is the causative organism in community acquired and ventilator associated pneumonia (CAP and VAP) and is also found in a high proportion of cystic fibrosis patients [22–26]. In the skin, imbalances in the skin microbiome resulting in *S. aureus* outgrowth are responsible for atopic dermatitis flares [27, 28]. The cellular mechanisms responsible for *S. aureus* pathogenesis in skin and lung epithelial cells are now well understood [27, 29, 30]. A key skin response to *S. aureus* is the interaction with toll-like receptor (TLR)-1, -2, and – 6 which recognise *S. aureus* cell wall lipopeptides and peptidoglycans [29]. Interaction of *S. aureus* with TLR-2 on keratinocytes can induce the production of neutrophil chemoattractants, such as IL-8, and antimicrobial peptides, including cathelicidin LL-37 together with beta defensins [29]. A key epithelial response to *S. aureus* and its associated virulence factors in the lung are dependent on TLR-2 signalling and inflammasome activation, to generate (pro-)inflammatory mediators, such as IL-1β, IL-6 and the neutrophil chemokine IL-8 [31].

To date, one paper demonstrates that exposure of mouse lungs through inhalation to 10mg/m^3 of CB for 4 days suppressed immune defence to the phagocytosis and removal of *S. aureus* 24 hours after exposure [32]. Recently Hussey and co-workers showed that 'black carbon' has significant effects on *S. aureus* biofilms and modifies the severity and invasiveness of infection *in vivo* [33]. Critically, there is a paucity of studies and models investigating the co-exposure of (nano)particles (*e.g.* CB) and an infectious agent (*e.g. S. aureus*). Such co-exposure studies would aim to model scenarios; i) of CB exposure on the background of an infection; ii) of resilience to infection having been exposed to CB. These scenarios are particularly relevant for the elderly, healthcare workers and occupational exposure across a variety of industries.

To address this gap in the literature the current work aims to develop a reproducible *in vitro* co-exposure model using CB and *S. aureus* as the test particle and infectious agent. Our working hypothesis for this study states that i) co-exposure responses can be determined in a cell culture system; and ii) that co-exposure to particle and pathogen leads to additive responses. This paper demonstrates the validity of considering experimental particle exposures under stressed and immunosuppressed conditions alongside those in healthy cells.

Results

Characterisation of CB

Firstly, we analysed CB alone and confirmed its physicochemical characteristics. SEM (Fig. 1) and TEM (Fig. 2) confirmed both the heterogeneous nature of the particles' morphology and the approximate size in the nanometre range. EDX spectroscopy (Supplementary Fig. 1) of CB detected a strong 'carbon' signal with minor contaminating peaks of silicon, sodium and chlorine, providing context as to the purity of the sample.

Next, CB size characteristics were assessed in biological media supporting bacterial and epithelial cell growth. Considering that bacterial and cell culture growth media contains significant added protein sources to support bacterial cell growth and metabolism and that previous work has suggested that soluble protein in media has a significant effect on nanoparticle physicochemical characteristics [34] the CB nanoparticles were characterised in deionised water, TSB (bacterial broth) and in 1% FBS / DMEM (cell culture media) through dynamic light scattering (Table 1). This confirmed that median particle diameter was significantly increased in TSB and 1%FBS / DMEM (531.2nm in both media at 100µg/ml CB) compared to water (458.7nm at 100µg/ml) at the same concentration. There was also evidence for particle aggregation as confirmed by higher PDI values, suggestive of higher heterogeneity, generated in particles suspended in TSB (0.418 at 10µg/ml) and 1% FBS / DMEM (0.362 at 10µg/ml) compared to water (0.246 at 10µg/ml).

Selection and optimisation of S. aureus strain for co-exposure

Our previous work confirmed that cellular immune responses to *S. aureus* (ability of neutrophils to kill and phagocytose) was strain dependent [35]. Therefore, to select an appropriate *S. aureus* strain, the same collection (Table 2) was added individually to human lung and skin epithelial cells and the inflammatory cytokine response assessed (Fig. 3). Infection of HaCaT skin and A549 lung epithelial cells with eight *S. aureus* strains demonstrated that *S. aureus* SH1000 consistently gave significantly higher inflammatory responses than the other strains tested. This was shown for IL-8 production in HaCaT skin epithelial cells (Fig. 3A) and A549 lung epithelial cells (Fig. 3B), and also IL-6 production in HaCaT skin epithelial cells (Supplementary Fig. 2). These results confirmed the selection of *S. aureus* SH1000 for further use in the current model.

Having selected an *S. aureus* strain with optimal cytokine induction properties its growth characteristics in 1% FBS/DMEM were confirmed for suitability in co-culture experiments. The growth of *S. aureus* SH1000 in deionised water, TSB and 1% FBS/DMEM was compared (Supplementary Fig. 3). It was clear that water would not support the growth of *S. aureus*, which showed a delayed logarithmic growth phase. In contrast growth in 1% FBS/DMEM showed a characteristic logarithmic growth phase (between 2–6 hours post inoculation) and a stationary phase (at greater than 9 hours post inoculation). Growth in 1% FBS/DMEM showed similar growth characteristics to that in staphylococcal bacterial broth, TSB. Since water did not sufficiently support the growth of *S. aureus* it was therefore not used for further study.

Effect of CB on S. aureus growth

The effect of CB (0-100μg/ml) on *S. aureus* SH1000 growth was investigated in 1% FBS/DMEM and in the staphylococcal growth media, TSB (Fig. 4). Preliminary experiments confirmed that concentrations of CB above 10μg/ml had significant absorbance (OD_{600}) that interfered with *S. aureus* growth assays (Supplementary Fig. 4). In 1% FBS/DMEM, CB (0–10μg/ml) caused a dose dependent decrease in the growth of *S. aureus* SH1000 by significantly reducing the level of maximum absorbance reached (Fig. 4A). In contrast, CB had very little effect on the growth of *S. aureus* SH1000 when grown in TSB (Fig. 4B).

This important observation showing that CB (0–10μg/ml) reduced growth of *S. aureus* in 1% FBS DMEM, was investigated by SEM to confirm if cellular toxicity could be observed (Fig. 5). SEM imaging clearly confirmed that CB alone (Fig. 5A) had a wide distribution of sizes (consistent with the DLS size measurements) and was subject to aggregation. Imaging of *S. aureus* SH1000 showed a typical ‘cocci’ (spherical) appearance as expected (Fig. 5B). SEM imaging of CB combined with *S. aureus* SH1000 (Fig. 5C), showed areas rich in binding between CB and bacteria. However, in those areas no evidence of toxicity, such as arrest of binary fission (two cells adhered with septum in place), surface crenulation (breakdown of cell membrane), decreases in cell size (dormancy) or cell lysis was seen. Indeed, the morphology of *S. aureus* SH1000 in areas rich in CB binding were no different to areas devoid of CB particles. Thus, the decreased growth was not due to toxicity.

Effect of CB and S. aureus SH1000 on (pro-)inflammatory responses in epithelial cells

To assess the (pro-)inflammatory response of human epithelial cells (skin and lung) to particle and bacteria, HaCaT and A549 epithelial cells were exposed to CB (0-100μg/ml) and *S. aureus* SH1000, alone and in combination for 5 and 24-hour incubation periods (Fig. 6). These exposure periods were consistent with the logarithmic and stationary phases of the *S. aureus* SH1000 growth (Fig. 3). Firstly, it was clear that CB alone (white bars) did not cause an increase in the constitutive production of IL-8 (left white bar) in HaCaT (Fig. 6A and B) or A549 (Fig. 6C and D) epithelial cells at 5 (Fig. 6A and C) or 24 hours (Fig. 6B and D). While constitutive IL-8 production increased between 5 and 24 hours (Fig. 6A vs 6B and 6C vs 6D) this only reached significance in A549 cells (Fig. 6C and D). In HaCaT skin epithelial cells at 5 hours *S. aureus* SH1000 alone (CB at 0μg/ml) significantly increased IL-8 production (Fig. 6A). In addition, the *S.*

aureus SH1000-induced IL-8, was dose dependently inhibited by the presence of CB, reaching significance at 100μg/ml (Fig. 6A). At 24 hours, significantly more IL-8 was produced in the presence of *S. aureus* SH1000 alone compared to 5 hours, but also with respect to the uninfected control at 24 hours. However, at 24 hours there was only partial inhibition of IL-8 by CB at 25μg/ml and this effect did not reach significance (Fig. 6B).

In comparison, A549 lung epithelial cells (Fig. 6C and D) showed a significant increase in IL-8 production in response to *S. aureus* SH1000 at 5 hours, compared to uninfected control (Fig. 6C, left white bar). By 24 hours, IL-8 was significantly enhanced in response to *S. aureus* SH1000 (Fig. 6D). Indeed, at 5 and 24 hours, *S. aureus* SH1000-induced IL-8 production in lung epithelial cells (Fig. 6C and D, black bars) was unaffected by CB over the concentration range studied with consistent significant increases compared to uninfected control at each dose of CB (Fig. 6C and D). In the same supernatants IL-6 and IL-10 were also measured by ELISA. IL-6 production was low, and no differences were detected between treatments (Supplementary Fig. 5) although *S. aureus* SH1000 induced IL-6 at 24 hours independently of CB dose (Supplementary Fig. 5B). IL-10 was undetectable in all cases (data not shown).

Finally, the production of the small antimicrobial peptide, human β2-defensin (hβD-2), was also determined in response to CB and *S. aureus* SH1000 (Fig. 7). At 5 hours, hβD-2 could not be detected in either HaCaT or A549 epithelial cells (data not shown). In contrast, at 24 hours, hβD-2, could be detected in supernatants from HaCaT (Fig. 7A) and A549 (Fig. 7B) epithelial cells. In both cell types, CB had no effect on constitutive hβD-2 production (left white bar) when given alone (white bars). When *S. aureus* SH1000 was given alone there was an increased production of hβD-2, compared to constitutive production, but the difference was not significant. In HaCaT but not A549 epithelial cells, *S. aureus* SH1000 combined with CB (100μg/ml) caused a significant increase in hβD-2 compared to *S. aureus* SH1000 alone (Fig. 7A). This confirms the ability to detect an antimicrobial peptide in this model system.

Discussion

The original aim of the current work was to establish an *in vitro* model whereby skin and lung epithelial cells could be co-exposed to a model particle and an infectious agent to enable their biological impact, namely immune responses, to be determined. It was reasoned that understanding cellular responses i) to a (nano)particle in the presence of an infection and ii) the response to infection during (nano)particle exposure is a poorly studied area of research and has implications to understanding such responses in immunosuppressed individuals. This goal was achieved by using HaCaT keratinocytes and A549 type II lung adenocarcinoma cells as the epithelial cells of choice due to their robust (pro-)inflammatory responses to a variety of stimuli and their resistance to injury [29, 36–38]. Carbon black (AROSPERSE® 15 thermal black powder, Evonik Degussa GmbH #BT10506621) was the (nano)particle used in the model due to its presence in a variety of everyday items, such as printer ink and rubber tyres. *S. aureus* was used as the infectious agent due to its importance in skin and lung infections, such as atopic dermatitis and pneumonia respectively. To the authors' knowledge this is one of the first demonstrations

of assessing immune parameters in a co-exposure system, where responses from eukaryotic (cytokines) and prokaryotic (growth) cells in co-culture have been determined following (nano)particle exposure.

Studying the effects of CB (nano)particles in immunosuppressed, immunocompromised and the elderly has been poorly studied, with most research focusing on 'healthy' cells prior to a cyto- or genotoxic stimulus [5, 39]. This work challenges that current dogma by studying CB (nano)particle exposure during infection with a human skin and lung pathogen, namely *S. aureus*. The major findings suggest that CB under certain circumstances can attenuate infection induced IL-8 and further enhance infection-induced hβD-2. Very few studies have addressed toxicity during infection. Hussey and colleagues showed that exposure to Black carbon (< 500nm, Sigma # 699632) particles can encourage invasion of *S. aureus* from the nasopharynx to the lower airways to establish infection [33]. In addition, nearly 20 years ago Jakab *et al*. confirmed that combinations of CB and formaldehyde or acrolein compromised lung host defence by suppressing killing and phagocytosis of *S. aureus* [32, 40]. Furthermore, recent studies of CB exposure in mice studied over 30 days confirm increased autophagy after 7 days which is reversible after 30 days [41, 42]. These studies and our own, confirm the importance of studying exposure to injured, stressed or infected cells.

SEM and TEM imaging confirmed the distribution of particle sizes assessed by DLS. While these results should be interpreted with caution due to measurement of dried material in the former and a suspension with the latter there is a good consistency in size estimation between the techniques. What was more striking was the dramatic effect of biological culture media on (nano)particle physicochemical properties, with increases in CB size following incubation in either the bacterial broth (TSB) or the cell culture media 1% FBS / DMEM. Although beyond the scope of this work, these results support previous work confirming the importance of 'protein corona' formation to the final biological activity of (nano)particles both *in vitro* and *in vivo* [43, 44]. Indeed, proteomic work suggests that the composition of the corona is not only dependent on the media, but also on the properties of the (nano)particle [45], as multi-walled carbon nanotubes (MWCNT) had different binding characteristics to CB [43]. It is clear however, that protein corona affects function, as bronchoalveolar lavage fluid (BALF) has been shown to enhance (nano)particle uptake and (pro-)inflammatory responses in primary human monocyte-derived macrophages [44].

The importance of media composition to provide specificity of function was clear during bacterial growth experiments. CB had no effect on *S. aureus* SH1000 growth when cultured in TSB bacterial broth. In contrast, 1% FBS / DMEM unmasked the inhibitory effects of CB on bacterial growth. The mechanism underlying this effect is unknown, however a simple explanation may be provided through 'nutrient restriction' [46–48]. With respect to protein content, TSB, contains tryptone, a digest of the protein casein and contains an assortment of peptides, while 1%FBS / DMEM contains much larger serum proteins, like bovine serum albumin (BSA). The former peptides are much more easily utilised for bacterial metabolism, unlike the larger BSA molecules which are more difficult to breakdown. Interestingly, BSA molecules have been shown to be part of protein corona formation in CB [49] and black carbon [50] and therefore may be sequestered away from the bacteria. Furthermore, others have suggested that many components of

serum bind to CB, including BSA, transferrin, apolipoprotein A-1 [51] and fibrinogen [52]. Therefore, our approach to model host, particle and pathogen in cell culture media should be considered when using advanced cell culture systems so that the established effects of 'adsorption artifacts' are considered [53].

One major achievement in this study was the successful detection of early induced cytokines (IL-8 and IL-6) and antimicrobial peptides (hβD-2). This is consistent with our previous studies using iron oxide nanoparticles in an epithelial / macrophage co-culture model [54]. In the current study, it was clear that early immune responses, defined by IL-8 production, were generated through *S. aureus* SH1000 stimulation, with an underlying modulation by CB which was time dependent. This is probably not that surprising given previous work showing that *S. aureus* stimulated cytokine and antimicrobial peptide responses in skin and lung epithelial cells and from patients [55–59]. The choice of cytokines and growth factors could be expanded in future work, to include the soluble pattern recognition 'collectin' molecules, metalloproteinases, chemokines such as CCL2 and regenerative growth factors such as TGFβ.

It has not escaped our attention that the CB dose of 100μg/ml when combined with *S. aureus* reduced IL-8 and increased hβD-2 production (compared to *S. aureus* alone) from HaCaT epithelial cells. While this result should be interpreted with caution as CB has been shown to interfere with some ELISA systems [60, 61] this result is fascinating and may be the first time this differential effect has been observed with this particle and pathogen combination. Interestingly, differential production of IL-8 / hβD-2 seems to be an evolving paradigm in barrier immunity as numerous authors report a similar effect but in anatomically distinct epithelial cell systems using different stimuli. Thus, *Cutibacterium acnes* (formerly *Propionibacterium acnes*) in skin keratinocytes [62], cigarette smoke in gingival epithelial cells [63] and *Streptococcus pneumoniae* in A549 cells [64] have all demonstrated IL-8 / hβD-2 immunomodulation. However, this effect seems even more important in the digestive tract where probiotics (*Lactobacillus rhamnosus* / *Bifidobacterium longum*) and *Pseudomonas aeruginosa* [65], 1,25-dihydroxyvitamin D3 or statins and *Salmonella typhimurium* [66, 67], and heat-killed probiotics (*L. casei* / *L. fermentum*) [68] have all shown similar mechanisms. Exposure at immune barriers is clearly important for determining successful immunity. The cellular signalling pathways underlying these effects are a clear target for future investigation.

The detailed cellular mechanism underlying the immunomodulatory action of CB remains open to interpretation. This is especially difficult to define given the number of potential interactions. Firstly, the role of serum proteins is important for final activity; this includes the proteins present but also their concentration. Indeed, it has been observed that differences in IL-8 output to CB if the concentration of serum is increased to 10% (compared to the 1% as used here). Secondly, SEM, TEM and DLS suggest that aggregation may also play a role in determining response. Indeed, previous studies in monocytes confirm CB particle size-dependent cytotoxicity [69]. Furthermore, it would be interesting to speculate whether the biphasic profile of IL-8 after 24 hours in HaCaT cells was due to particle size and / or aggregation. Thirdly, determination of the cellular targets of CB is vital. Indeed, Vuong and co-workers provide compelling data confirming the particle specific effects of CB in proteomic responses associated with cell

death and proliferation pathways in A549 cells [70]. There is also evidence that CB has the potential to bind certain cytokines to influence biological activity [71] or interfere with ELISA technologies [60, 61].

The move to study co-exposures is challenging but much more relevant to human pathology and small adaptions in the current model could apply to numerous other particulate and infectious diseases. These include but are not limited to co-infection with influenza and *S. aureus* in the lung [72, 73] where a model has recently been considered [74]; exposure of cigarette smoke (passive smoking) and respiratory syncytial virus (RSV) in the lung [75]; human bacterial and viral coinfections with respiratory syncytial viruses [76] not to mention exposures to particles such as titanium, sulphur dioxide and ozone.

While this study is an advance in host, pathogen and particle model systems there are also limitations. Firstly, the full mechanisms of CB based immunomodulation was beyond the scope of this work. Secondly, bacterial growth was measured by optical density alone and future work should incorporate a viable count to increase sensitivity. Thirdly, a more equal balance of inflammatory response between pathogen and particle may help further address the mechanism of CB cellular interaction. Finally, our study did not allow further estimation of the safe exposure limits for CB. However, they have been defined on the skin, when used as a colourant, of 20nm minimum size, and a concentration up to 10% [77]. Limits for lung exposure have been discussed recently [8] and suggest a no-observational-exposure-limit (NOEL) of 1mg/m^3 and a LOEL of 7-50mg/m^3 depending on the surface area. However, doses are hard to extrapolate to humans because of the significantly greater surface area of the skin and lungs.

In conclusion, this work confirms the development of a pathogen and particle co-exposure model in human skin and lung epithelial cells. Studying particle exposure under stressed, pathological or infected conditions as compared to traditional exposure in ‘healthy’ cells is a vital addition to the nanotoxicology assessment toolkit.

Materials And Methods

Bacterial strains and routine culture of S. aureus

Six clinical methicillin resistant isolates obtained from human bronchoalveolar alveolar lavage fluid (BAL) were used [35, 78]. In addition, two control strains; *S. aureus*, SH1000 and *S. aureus* Cowan 1 ([79–84] and Table 2) were used. For culture, one single colony of *S. aureus* was taken from an agar plate and inoculated into 5ml of sterile tryptic soy broth (TSB), then grown overnight at 37°C. The overnight cultures were standardised to OD_{600} = 0.1 (~ 1 × 10^8 cfu/ml).

Preparation and characterisation of Carbon Black (CB)

CB dose preparation

CB, AROSPERSE® 15 thermal black powder (Evonik Degussa GmbH #BT10506621) was weighed out at 1mg using the OHAUS Explorer Semi-Micro Balance housed in a WAYSAFE (#GP1540) to 1ml of the

selected media (ultra-pure H_2O, Tryptic soy broth (TSB) or 1% FBS/DMEM). This suspension was vortexed for 1 minute and sonicated in a 90W Ultrasonic water bath (Fisher Scientific #FB15046) at maximum power for approximately 30–40 minutes to ensure the CB was completely suspended. CB was then diluted to specific doses (including 0, 2, 4, 8, 10, 25, 50, 100 µg/ml) in water, TSB, 1% FBS / DMEM.

Zetasizer

Agglomerate medial and size distribution of CB samples was determined by dynamic light scattering (DLS) using a Malvern Zeta-Sizer Nano ZS (Malvern instruments Ltd., UK). Measurements were performed in deionised water, TSB and 1% FBS DMEM and presented as an average of 10 readings, with samples briefly vortexed and incubated at 37°C prior to measurements.

Transmission electron microscopy (TEM)

TEM was used to analyse CB particle size, shape, morphology, crystallinity and purity. A drop of diluted material (50 µg/ml in double distilled H_2O) was drop-cast on a copper TEM grid coated with a continuous carbon film (Agar Scientific, UK) and left to air dry. TEM analysis was undertaken with a FEI Talos F200x G2 TEM (ThermoFisher Scientific, UK) operating at 200 kV and fitted with a high angle annular dark field (HAADF) detector, a Gatan Orius SC600A CCD camera, and an Oxford Instruments 80mm^2 silicon drift energy-dispersive X-ray (EDX) spectrometer. Images were taken from 20 areas at magnifications between x7000 and x40000 with a dwell time of 10 µs.

S. aureus growth with CB

Standardised suspensions of *S. aureus* SH1000 were prepared as above but diluted to twice (2X) their final concentrations in water, TSB or 1%FBS/DMEM. Likewise, CB was also prepared at twice the concentration used (0, 4, 8, 16, 20, 50, 100 and 200µg/ml). Then using a 96 well plate, 100µL of diluted standardised *S. aureus* and 100µl of the double concentrated CB were combined (to generate the defined concentration) and left to incubate at 37°C at 200rpm for either 5 or 24 hours. Then the OD_{600} was read every hour, with constant oscillations (100 rpm), using the FLUOstar Omega microplate reader (BMG Labtech, Germany) for up to 24 hours. Preliminary experiments confirmed that CB at doses below 25µg/ml did not interfere with the measurement of absorbance (OD600nm) using the microplate reader (Supplementary Fig. 4)

Preparation of CB and S. aureus for SEM

Bacterial and CB suspensions were prepared as previously described above and then bound to Thermanox disks. Briefly, pre-sterilised Nunc™ Thermanox™ Coverslips (13mm diameter, Thermo Scientific, Paisley, UK) were taped onto a glass microscope slide and placed in a cytospin filter cartridge. Suspensions were mixed gently before 80 µl was pipetted into the cytospin cartridges prior to centrifugation at 112g for 3 minutes in a Shandon Cytospin 3. The cartridges were then taken apart and the Thermanox™ disk removed carefully. The samples were then left to air-dry overnight before being

fixed with 2.5% glutaraldehyde in 0.1M piperazine-N,N'-bis(2-ethanesulfonic acid (PIPES), pH 7.4 for 5 min, post-fixed with 1% osmium tetroxide (OsO4; Simec Trade AG, Zofingen, Switzerland) in 0.1M PIPES (pH 6.8) for 1 h, dehydrated through an ethanol series (50%, 70%, 96%, 100%, 5 min each step) and an ethanol: hexamethyldisilazane (HMDS) series (2:1, 1:1, 1:2, for 5 min each step), and finally in 100% HMDS for 5min. Samples were then left to air-dry overnight, mounted on stubs and viewed with a Hitachi S4800 High resolution Scanning electron microscope using the upper secondary electron (SE) detector with a − 10 V or -20 V bias to minimise SE detection and maximise backscattered electron (BSE) detection, at an acceleration voltage of 1 kV and emission current of 10 µA. Images were taken from 10 random areas of the sample.

Cell culture

The choice of cells was determined by the major route of exposure for CB, namely skin and lung. Likewise, the lung and skin form the major sites for *S. aureus* pathogenesis. Therefore, epithelial cell lines from skin and lung were used in this study. HaCaT immortalized human keratinocytes, and A549 adenocarcinoma Type II human alveolar epithelial cells were used [85, 86]. Both cell lines were grown in Dulbecco's, minimum essential medium (DMEM) supplemented with 10% fetal bovine serum (FBS), 1% penicillin (100µg/ml) / streptomycin (100U/ml), 1% glutamine (2mM) and incubated at 37°C / 5% CO_2. HaCaT and A549s were sub-cultured at 90% confluence with TrypLE Express according to manufacturer's instructions. Cell viability was assessed by trypan blue (0.2%) exclusion.

S. aureus infection of epithelial cells

A 10X standardised suspension of *S. aureus* SH1000 was prepared following overnight pre-culture (OD_{600} = 1.0, ~ 1 x10^9/ml). Replicate 24 well plates were seeded with 50,000 epithelial cells / well in a total volume of 1ml cell culture media. The plates were then incubated at 37°C in a 5% CO_2 environment for 24 hours. Then, the following day media was removed and replaced with 995µl of DMEM supplemented with 1% FBS and L-glutamine (without antibiotics). Then, 5 µl (~ 5 x 10^6 bacteria) of 10X standardised *S. aureus* SH1000 were added before the plate was incubated for either 5 or 24 hours at 37°C in a 5% CO_2 environment. Then the media was removed and decanted into a clean Eppendorf and centrifuged at 8064g for 5 mins. After centrifugation, 900µl of the supernatant was removed without dislodging the pellet and aliquoted into a clean Eppendorf before being placed in a -80 freezer for storage until ELISA determination could occur.

Co-exposure of epithelial cells to S. aureus and CB

Epithelial cell monolayers and *S. aureus* were prepared as previously described for infection studies with *S. aureus* SH1000 alone, except the following day media was removed and replaced with 495µl of DMEM supplemented with 1% FBS and L-glutamine (without antibiotics). Then, 5 µl (~ 5 x 10^6 bacteria) of 10X standardised *S. aureus* SH1000 and 500 µl of CB dilutions (0-200µg/ml) were added before the plate was incubated for either 5 or 24 hours at 37°C in a 5% CO_2. The media was then removed and decanted into a

clean Eppendorf and centrifuged at 8064g for 5 mins. After centrifugation, 900µl of the supernatant was removed without dislodging the pellet and aliquoted into a clean Eppendorf before being placed in a -80 freezer for storage until ELISA determination could occur.

Enzyme linked immunosorbent assay (ELISA)

DuoSet ELISA (R&D Systems, Abingdon, UK) for human IL-8, IL-6 and IL-10 were carried out according to the manufacturers' instructions. Human β-Defensin-2 (hβD-2) ELISA was assayed using a TMB development kit (PeproTech, London, UK) according to the manufacturer's instructions.

Data and statistical analysis

Growth and cytokine data were presented as the mean ± standard error of the mean (SEM). A minimum of 3 biological repeats were conducted for all analyses presented. GraphPad Prism software (Version 9.1.2) was used for statistical analysis using a one-way ANOVA parametric test, including a Sidak *post hoc* test for multiple pairwise comparisons with $*p \leq 0.05$ being considered significant.

Declarations

Ethics approval and consent to participate

Not applicable in this study

Consent for publication

Not applicable in this study

Availability of data and materials

The datasets are available from the corresponding author upon reasonable request

Competing interests

To our knowledge none of the authors have any competing interests.

Funding

The work was part-funded by a studentship to SB from SUMS.

Authors' contributions

Author contributions are as follows; SB performed the experiments. SJE and MJB supported the particle characterisation experiments. LGH performed the SEM and edited the manuscript. REJ supported the microbiology and read the manuscript. SHD read and edited the manuscript. TSW and MJDC were responsible for the conceptual design of experiments. TSW drafted the manuscript.

Acknowledgements

We would like to thank Prof Richard Palmer and Dr Yubiao Niu for training and access to the TEM located in the Advanced Imaging of Materials (AIM) facility at Swansea University.

References

1. Al-Hartomy OA, Al-Solamy F, Al-Ghamdi A, Dishovsky N, Ivanov M, Mihaylov M, El-Tantawy F. Influence of Carbon Black Structure and Specific Surface Area on the Mechanical and Dielectric Properties of Filled Rubber Composites. International Journal of Polymer Science. 2011;2011:521985.
2. Surovikin YV, Shaitanov AG, Resanov IV, Syr'eva AV. The Properties of Nanodispersed Carbon Black Particles After Thermal Treatment. Procedia Eng. 2015;113:519–24.
3. Robertson CG, Hardman NJ. **Nature of Carbon Black Reinforcement of Rubber: Perspective on the Original Polymer Nanocomposite**. *Polymers (Basel)* 2021, 13.
4. Arduini F, Cinti S, Mazzaracchio V, Scognamiglio V, Amine A, Moscone D. Carbon black as an outstanding and affordable nanomaterial for electrochemical (bio)sensor design. Biosens Bioelectron. 2020;156:112033.
5. Stone V, Miller MR, Clift MJD, Elder A, Mills NL, Moller P, Schins RPF, Vogel U, Kreyling WG, Alstrup Jensen K, et al. Nanomaterials Versus Ambient Ultrafine Particles: An Opportunity to Exchange Toxicology Knowledge. Environ Health Perspect. 2017;125:106002.
6. Yong M, Anderle L, Levy L, McCunney RJ. Carbon Black and Lung Cancer Mortality-A Meta-regression Analysis Based on Three Occupational Cohort Studies. J Occup Environ Med. 2019;61:949–940.
7. World Health Organisation IAfRoC. **IARC monographs on the evaluation of carcinogenic risks to humans: Carbon Black, Titanium Dioxide and Talc**. vol. 93; 2010.
8. Chaudhuri I, Fruijtier-Polloth C, Ngiewih Y, Levy L. Evaluating the evidence on genotoxicity and reproductive toxicity of carbon black: a critical review. Crit Rev Toxicol. 2018;48:143–69.
9. Holz O, Heusser K, Muller M, Windt H, Schwarz K, Schindler C, Tank J, Hohlfeld JM, Jordan J. Airway and systemic inflammatory responses to ultrafine carbon black particles and ozone in older healthy subjects. J Toxicol Environ Health A. 2018;81:576–88.
10. Bennett BA, Mitzner W, Tankersley CG. The effects of age and carbon black on airway resistance in mice. Inhal Toxicol. 2012;24:931–8.
11. Hamade AK, Misra V, Rabold R, Tankersley CG. Age-related changes in cardiac and respiratory adaptation to acute ozone and carbon black exposures: interstrain variation in mice. Inhal Toxicol. 2010;22(Suppl 2):84–94.
12. Schraufnagel DE. The health effects of ultrafine particles. Exp Mol Med. 2020;52:311–7.
13. Herzog E, Casey A, Lyng FM, Chambers G, Byrne HJ, Davoren M. A new approach to the toxicity testing of carbon-based nanomaterials–the clonogenic assay. Toxicol Lett. 2007;174:49–60.

14. Monteiller C, Tran L, MacNee W, Faux S, Jones A, Miller B, Donaldson K. The pro-inflammatory effects of low-toxicity low-solubility particles, nanoparticles and fine particles, on epithelial cells in vitro: the role of surface area. Occup Environ Med. 2007;64:609–15.
15. Totsuka Y, Higuchi T, Imai T, Nishikawa A, Nohmi T, Kato T, Masuda S, Kinae N, Hiyoshi K, Ogo S, et al. Genotoxicity of nano/microparticles in in vitro micronuclei, in vivo comet and mutation assay systems. Part Fibre Toxicol. 2009;6:23.
16. Horie M, Kato H, Endoh S, Fujita K, Komaba LK, Nishio K, Nakamura A, Miyauchi A, Yamamoto K, Kinugasa S, et al. Cellular effects of industrial metal nanoparticles and hydrophilic carbon black dispersion. J Toxicol Sci. 2014;39:897–907.
17. Barlow PG, Clouter-Baker A, Donaldson K, Maccallum J, Stone V. Carbon black nanoparticles induce type II epithelial cells to release chemotaxins for alveolar macrophages. Part Fibre Toxicol. 2005;2:11.
18. Barlow PG, Donaldson K, MacCallum J, Clouter A, Stone V. Serum exposed to nanoparticle carbon black displays increased potential to induce macrophage migration. Toxicol Lett. 2005;155:397–401.
19. Findlay F, Pohl J, Svoboda P, Shakamuri P, McLean K, Inglis NF, Proudfoot L, Barlow PG. Carbon Nanoparticles Inhibit the Antimicrobial Activities of the Human Cathelicidin LL-37 through Structural Alteration. J Immunol. 2017;199:2483–90.
20. Bennett MR, Thomsen IP. **Epidemiological and Clinical Evidence for the Role of Toxins in S. aureus Human Disease**. *Toxins (Basel)* 2020, 12.
21. Balasubramanian D, Harper L, Shopsin B, Torres VJ. **Staphylococcus aureus pathogenesis in diverse host environments**. *Pathog Dis* 2017, 75.
22. Jean SS, Chang YC, Lin WC, Lee WS, Hsueh PR, Hsu CW. **Epidemiology, Treatment, and Prevention of Nosocomial Bacterial Pneumonia**. *J Clin Med* 2020, 9.
23. Shoar S, Musher DM. Etiology of community-acquired pneumonia in adults: a systematic review. Pneumonia (Nathan). 2020;12:11.
24. Ranzani OT, Motos A, Chiurazzi C, Ceccato A, Rinaudo M, Li Bassi G, Ferrer M, Torres A. Diagnostic accuracy of Gram staining when predicting staphylococcal hospital-acquired pneumonia and ventilator-associated pneumonia: a systematic review and meta-analysis. Clin Microbiol Infect. 2020;26:1456–63.
25. Hurley MN, Smyth AR. Staphylococcus aureus in cystic fibrosis: pivotal role or bit part actor? Curr Opin Pulm Med. 2018;24:586–91.
26. Blanchard AC, Waters VJ. Microbiology of Cystic Fibrosis Airway Disease. Semin Respir Crit Care Med. 2019;40:727–36.
27. Geoghegan JA, Irvine AD, Foster TJ. Staphylococcus aureus and Atopic Dermatitis: A Complex and Evolving Relationship. Trends Microbiol. 2018;26:484–97.
28. Ogonowska P, Gilaberte Y, Baranska-Rybak W, Nakonieczna J. Colonization With Staphylococcus aureus in Atopic Dermatitis Patients: Attempts to Reveal the Unknown. Front Microbiol. 2020;11:567090.

29. Bitschar K, Wolz C, Krismer B, Peschel A, Schittek B. Keratinocytes as sensors and central players in the immune defense against Staphylococcus aureus in the skin. J Dermatol Sci. 2017;87:215–20.
30. Pivard M, Moreau K, Vandenesch F. **Staphylococcus aureus Arsenal To Conquer the Lower Respiratory Tract**. *mSphere* 2021, 6.
31. Perret M, Badiou C, Lina G, Burbaud S, Benito Y, Bes M, Cottin V, Couzon F, Juruj C, Dauwalder O, et al. Cross-talk between Staphylococcus aureus leukocidins-intoxicated macrophages and lung epithelial cells triggers chemokine secretion in an inflammasome-dependent manner. Cell Microbiol. 2012;14:1019–36.
32. Jakab GJ. The toxicologic interactions resulting from inhalation of carbon black and acrolein on pulmonary antibacterial and antiviral defenses. Toxicol Appl Pharmacol. 1993;121:167–75.
33. Hussey SJK, Purves J, Allcock N, Fernandes VE, Monks PS, Ketley JM, Andrew PW, Morrissey JA. Air pollution alters Staphylococcus aureus and Streptococcus pneumoniae biofilms, antibiotic tolerance and colonisation. Environ Microbiol. 2017;19:1868–80.
34. Kopac T. Protein corona, understanding the nanoparticle-protein interactions and future perspectives: A critical review. Int J Biol Macromol. 2021;169:290–301.
35. Evans SJ, Roberts AEL, Morris AC, Simpson AJ, Harris LG, Mack D, Jenkins RE, Wilkinson TS. Contrasting effects of linezolid on healthy and dysfunctional human neutrophils: reducing C5a-induced injury. Sci Rep. 2020;10:16377.
36. Ruaro B, Salton F, Braga L, Wade B, Confalonieri P, Volpe MC, Baratella E, Maiocchi S, Confalonieri M. **The History and Mystery of Alveolar Epithelial Type II Cells: Focus on Their Physiologic and Pathologic Role in Lung**. *Int J Mol Sci* 2021, 22.
37. Hiemstra PS, McCray PB Jr, Bals R. The innate immune function of airway epithelial cells in inflammatory lung disease. Eur Respir J. 2015;45:1150–62.
38. Jiang Y, Tsoi LC, Billi AC, Ward NL, Harms PW, Zeng C, Maverakis E, Kahlenberg JM, Gudjonsson JE. **Cytokinocytes: the diverse contribution of keratinocytes to immune responses in skin**. *JCI Insight* 2020, 5.
39. Clift MJD, Jenkins GJS, Doak SH. An Alternative Perspective towards Reducing the Risk of Engineered Nanomaterials to Human Health. Small. 2020;16:e2002002.
40. Jakab GJ, Risby TH, Hemenway DR. **Use of physical chemistry and in vivo exposure to investigate the toxicity of formaldehyde bound to carbonaceous particles in the murine lung**. *Res Rep Health Eff Inst* 1992:1–39, discussion 41 – 39.
41. He W, Peng H, Ma J, Wang Q, Li A, Zhang J, Kong H, Li Q, Sun Y, Zhu Y. Autophagy changes in lung tissues of mice at 30 days after carbon black-metal ion co-exposure. Cell Prolif. 2020;53:e12813.
42. Kong H, Xia K, Pan L, Zhang J, Luo Y, Y Z, Ciu Z, El-Sayed NN, Aladalbahi A, Chen N, et al. Autophagy and lysosomal dysfunction: A new insight into mechanism of synergistic pulmonary toxicity of carbon black-metal ions co-exposure. Carbon. 2017;111:322–33.
43. Cai X, Ramalingam R, Wong HS, Cheng J, Ajuh P, Cheng SH, Lam YW. Characterization of carbon nanotube protein corona by using quantitative proteomics. Nanomedicine. 2013;9:583–93.

44. Shaw CA, Mortimer GM, Deng ZJ, Carter ES, Connell SP, Miller MR, Duffin R, Newby DE, Hadoke PW, Minchin RF. Protein corona formation in bronchoalveolar fluid enhances diesel exhaust nanoparticle uptake and pro-inflammatory responses in macrophages. Nanotoxicology. 2016;10:981–91.
45. Hirsch V, Kinnear C, Moniatte M, Rothen-Rutishauser B, Clift MJ, Fink A. Surface charge of polymer coated SPIONs influences the serum protein adsorption, colloidal stability and subsequent cell interaction in vitro. Nanoscale. 2013;5:3723–32.
46. Brown SA, Palmer KL, Whiteley M. Revisiting the host as a growth medium. Nat Rev Microbiol. 2008;6:657–66.
47. Krismer B, Liebeke M, Janek D, Nega M, Rautenberg M, Hornig G, Unger C, Weidenmaier C, Lalk M, Peschel A. Nutrient limitation governs Staphylococcus aureus metabolism and niche adaptation in the human nose. PLoS Pathog. 2014;10:e1003862.
48. Monod J. The growth of bacterial culture. Annual Rev Micro. 1949;3:371–94.
49. Chen TT, Chuang KJ, Chiang LL, Chen CC, Yeh CT, Wang LS, Gregory C, Jones T, BeruBe K, Lee CN, et al. Characterization of the interactions between protein and carbon black. J Hazard Mater. 2014;264:127–35.
50. Wu H, Chen M, Shang M, Li X, Mu K, Fan S, Jiang S, Li W. Insights into the binding behavior of bovine serum albumin to black carbon nanoparticles and induced cytotoxicity. Spectrochim Acta A Mol Biomol Spectrosc. 2018;200:51–7.
51. Fertsch-Gapp S, Semmler-Behnke M, Wenk A, Kreyling WG. Binding of polystyrene and carbon black nanoparticles to blood serum proteins. Inhal Toxicol. 2011;23:468–75.
52. Ruh H, Kuhl B, Brenner-Weiss G, Hopf C, Diabate S, Weiss C. Identification of serum proteins bound to industrial nanomaterials. Toxicol Lett. 2012;208:41–50.
53. Val S, Hussain S, Boland S, Hamel R, Baeza-Squiban A, Marano F. Carbon black and titanium dioxide nanoparticles induce pro-inflammatory responses in bronchial epithelial cells: need for multiparametric evaluation due to adsorption artifacts. Inhal Toxicol. 2009;21(Suppl 1):115–22.
54. Evans SJ, Clift MJD, Singh N, Wills JW, Hondow N, Wilkinson TS, Burgum MJ, Brown AP, Jenkins GJ, Doak SH. In vitro detection of in vitro secondary mechanisms of genotoxicity induced by engineered nanomaterials. Part Fibre Toxicol. 2019;16:8.
55. Kang SS, Kim SK, Baik JE, Ko EB, Ahn KB, Yun CH, Han SH. Staphylococcal LTA antagonizes the B cell-mitogenic potential of LPS. Sci Rep. 2018;8:1496.
56. Cho JW, Cho SY, Lee KS. Roles of SEA-expressing Staphylococcus aureus, isolated from an atopic dermatitis patient, on expressions of human beta-defensin-2 and inflammatory cytokines in HaCaT cells. Int J Mol Med. 2009;23:331–5.
57. Sorrentino R, de Souza PM, Sriskandan S, Duffin C, Paul-Clark MJ, Mitchell JA. Pattern recognition receptors and interleukin-8 mediate effects of Gram-positive and Gram-negative bacteria on lung epithelial cell function. Br J Pharmacol. 2008;154:864–71.
58. Cheon IS, Woo SS, Kang SS, Im J, Yun CH, Chung DK, Park DK, Han SH. Peptidoglycan-mediated IL-8 expression in human alveolar type II epithelial cells requires lipid raft formation and MAPK

activation. Mol Immunol. 2008;45:1665–73.

59. Rath S, Ziesemer S, Witte A, Konkel A, Muller C, Hildebrandt P, Volker U, Hildebrandt JP. S. aureus haemolysin A-induced IL-8 and IL-6 release from human airway epithelial cells is mediated by activation of p38- and Erk-MAP kinases and additional, cell type-specific signalling mechanisms. Cell Microbiol. 2013;15:1253–65.
60. Kroll A, Pillukat MH, Hahn D, Schnekenburger J. Current in vitro methods in nanoparticle risk assessment: limitations and challenges. Eur J Pharm Biopharm. 2009;72:370–7.
61. Kroll A, Pillukat MH, Hahn D, Schnekenburger J. Interference of engineered nanoparticles with in vitro toxicity assays. Arch Toxicol. 2012;86:1123–36.
62. Nagy I, Pivarcsi A, Koreck A, Szell M, Urban E, Kemeny L. Distinct strains of Propionibacterium acnes induce selective human beta-defensin-2 and interleukin-8 expression in human keratinocytes through toll-like receptors. J Invest Dermatol. 2005;124:931–8.
63. Mahanonda R, Sa-Ard-Iam N, Eksomtramate M, Rerkyen P, Phairat B, Schaecher KE, Fukuda MM, Pichyangkul S. Cigarette smoke extract modulates human beta-defensin-2 and interleukin-8 expression in human gingival epithelial cells. J Periodontal Res. 2009;44:557–64.
64. Lin L, Wen SH, Guo SZ, Su XY, Wu HJ, Chong L, Zhang HL, Zhang WX, Li CC. Role of SIRT1 in Streptococcus pneumoniae-induced human beta-defensin-2 and interleukin-8 expression in A549 cell. Mol Cell Biochem. 2014;394:199–208.
65. Huang FC, Lu YT, Liao YH. Beneficial effect of probiotics on Pseudomonas aeruginosa-infected intestinal epithelial cells through inflammatory IL-8 and antimicrobial peptide human beta-defensin-2 modulation. Innate Immun. 2020;26:592–600.
66. Huang FC. The differential effects of 1,25-dihydroxyvitamin D3 on Salmonella-induced interleukin-8 and human beta-defensin-2 in intestinal epithelial cells. Clin Exp Immunol. 2016;185:98–106.
67. Huang FC, Huang SC. **Differential Effects of Statins on Inflammatory Interleukin-8 and Antimicrobial Peptide Human Beta-Defensin 2 Responses in Salmonella-Infected Intestinal Epithelial Cells**. *Int J Mol Sci* 2018, 19.
68. Habil N, Abate W, Beal J, Foey AD. Heat-killed probiotic bacteria differentially regulate colonic epithelial cell production of human beta-defensin-2: dependence on inflammatory cytokines. Benef Microbes. 2014;5:483–95.
69. Sahu D, Kannan GM, Vijayaraghavan R. Carbon black particle exhibits size dependent toxicity in human monocytes. Int J Inflam. 2014;2014:827019.
70. Vuong NQ, Goegan P, Mohottalage S, Breznan D, Ariganello M, Williams A, Elisma F, Karthikeyan S, Vincent R, Kumarathasan P. Proteomic changes in human lung epithelial cells (A549) in response to carbon black and titanium dioxide exposures. J Proteomics. 2016;149:53–63.
71. Seagrave J, Knall C, McDonald JD, Mauderly JL. Diesel particulate material binds and concentrates a proinflammatory cytokine that causes neutrophil migration. Inhal Toxicol. 2004;16(Suppl 1):93–8.
72. Wilden JJ, Jacob JC, Ehrhardt C, Ludwig S, Boergeling Y. **Altered Signal Transduction in the Immune Response to Influenza Virus and S. pneumoniae or S. aureus Co-Infections**. *Int J Mol Sci* 2021, 22.

73. McDanel JS, Perencevich EN, Storm J, Diekema DJ, Herwaldt L, Johnson JK, Winokur PL, Schweizer ML. Increased Mortality Rates Associated with Staphylococcus aureus and Influenza Co-infection, Maryland and Iowa, USA(1). Emerg Infect Dis. 2016;22:1253–6.
74. Bruchhagen C, van Kruchten A, Klemm C, Ludwig S, Ehrhardt C. In Vitro Models to Study Influenza Virus and Staphylococcus aureus Super-Infection on a Molecular Level. Methods Mol Biol. 2018;1836:375–86.
75. DiFranza JR, Masaquel A, Barrett AM, Colosia AD, Mahadevia PJ. Systematic literature review assessing tobacco smoke exposure as a risk factor for serious respiratory syncytial virus disease among infants and young children. BMC Pediatr. 2012;12:81.
76. Pacheco GA, Galvez NMS, Soto JA, Andrade CA, Kalergis AM. **Bacterial and Viral Coinfections with the Human Respiratory Syncytial Virus**. *Microorganisms* 2021, 9.
77. Scientific Committee On. Consumer S, Chaudhry Q. Opinion of the Scientific Committee on Consumer safety (SCCS) - Second revision of the opinion on carbon black, nano-form, in cosmetic products. Regul Toxicol Pharmacol 2016, 79:103–4.
78. Conway Morris A, Kefala K, Wilkinson TS, Dhaliwal K, Farrell L, Walsh T, Mackenzie SJ, Reid H, Davidson DJ, Haslett C, et al. C5a mediates peripheral blood neutrophil dysfunction in critically ill patients. Am J Respir Crit Care Med. 2009;180:19–28.
79. Horsburgh MJ, Aish JL, White IJ, Shaw L, Lithgow JK, Foster SJ. sigmaB modulates virulence determinant expression and stress resistance: characterization of a functional rsbU strain derived from Staphylococcus aureus 8325-4. J Bacteriol. 2002;184:5457–67.
80. O'Neill AJ. Staphylococcus aureus SH1000 and 8325-4: comparative genome sequences of key laboratory strains in staphylococcal research. Lett Appl Microbiol. 2010;51:358–61.
81. Cowan ST. The classification of staphylococci by precipitation and biological reactions. J Path Bact. 1938;46:31–45.
82. Cowan ST. The classification of staphylococci by slide agglutination. J Path Bact. 1939;48:169–73.
83. Cowan ST. Staphylococcal infection in rabbits: antibacterial and non-specific immunity. J Path Bact. 1939;48:545–55.
84. Christie R, Keogh EV. Physiological and serological characteristics of staphylococci of human origin. J Path Bact. 1940;51:189–97.
85. Boukamp P, Petrussevska RT, Breitkreutz D, Hornung J, Markham A, Fusenig NE. Normal keratinization in a spontaneously immortalized aneuploid human keratinocyte cell line. J Cell Biol. 1988;106:761–71.
86. Lieber M, Smith B, Szakal A, Nelson-Rees W, Todaro G. A continuous tumor-cell line from a human lung carcinoma with properties of type II alveolar epithelial cells. Int J Cancer. 1976;17:62–70.

Tables

Table 1: Carbon Black nanoparticle physicochemical parameters in aqueous media.

Carbon Black (AROSPERSE® 15) at final concentrations of 4, 10, 25, 50 and 100µg/ml were suspended in deionised water, 1%FBS DMEM, and TSB, prior to analysis by Zetasizer. Parameters measured include size (nm), median particle population size (nm), hydrodynamic radius (nm) and the polydispersity index (PDI).

Carbon Black (mg/ml)	Dispersant / Solvent	Size range (nm)	Median size population (nm)	Z-average (nm)	Polydispersal index
4	Water	220.0 – 615.0	342	436.8	0.331
10	Water	164.2 – 955.4	396.1	422.9	0.246
25	Water	190.1 – 5560.0	487.7	409.9	0.190
50	Water	141.8 – 5560.0	396.1	405.9	0.175
100	Water	164.2 – 6439.0	458.7	410.4	0.165
4	TSB	255.0 – 712.0	342.0	635.3	0.546
10	TSB	255.0 – 825.0	396.1	625.5	0.418
25	TSB	220.2 – 955.4	458.7	610.9	0.327
50	TSB	295.3 – 825.0	458.7	644.5	0.383
100	TSB	295.3 – 1106.0	531.2	669.6	0.319
4	DMEM with 1% FBS	220.2 – 825.0	396.1	509.8	0.398
10	DMEM with 1% FBS	190.1 – 955.4	396.1	530.2	0.362
25	DMEM with 1% FBS	220.2 – 1106.0	458.7	518.8	0.251
50	DMEM with 1% FBS	220.2 – 1281.1	531.2	529.9	0.223
100	DMEM with 1% FBS	220.2 – 1281.1	531.2	511.8	0.163

Table 2: Strains of *S. aureus* used in this study.

Eight *S. aureus* strains were used in this study. They included two reference strains and six strains clinically defined as VAP or non-VAP from a previous study.

S. aureus strain	Source	Reference
SH1000	Reference / Control	[35,78]
Cowan 1	Reference / Control ATCC 12598 / NCTC 8530	[81-84]
VAP 25	Human BAL	[35, 78]
VAP 26	Human BAL	[35, 78]
VAP 32	Human BAL	[35, 78]
VAP 34	Human BAL	[35, 78]
VAP 39	Human BAL	[35, 78]
VAP 40	Human BAL	[35, 78]

Figures

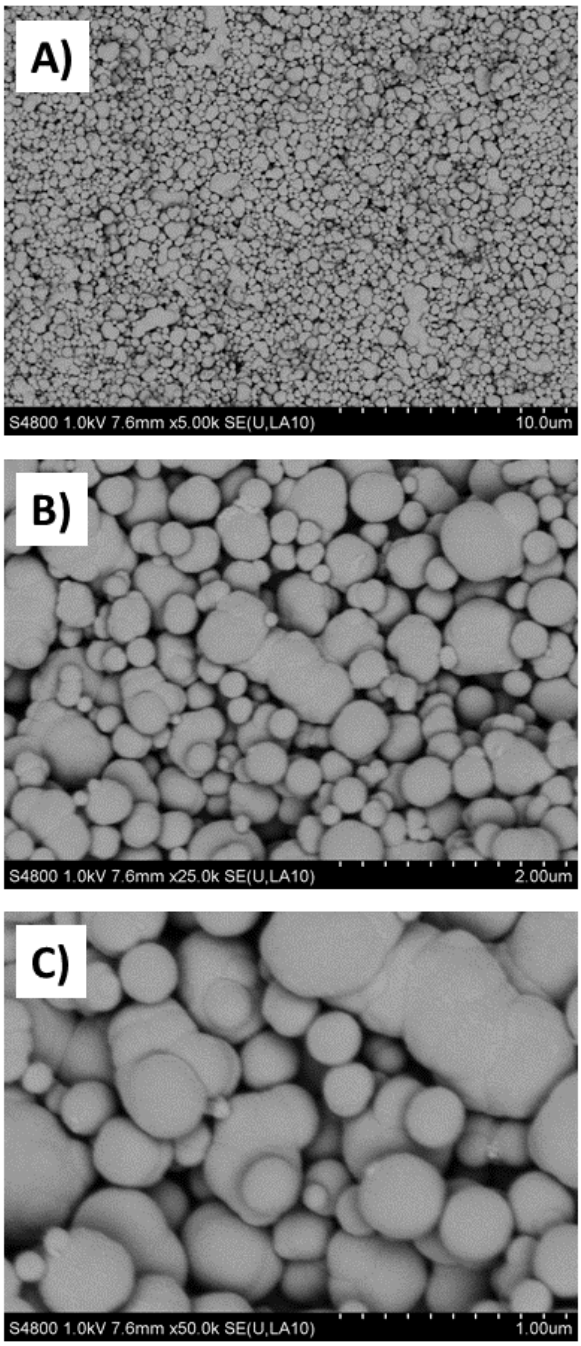

Figure 1

SEM imaging of Carbon Black. Carbon Black (AROSPERSE® 15) was imaged with a Hitachi S4800 SEM microscope at increasing resolution (A-C). Particles appeared spherical in shape with clear diversity in particle size. Size scale shown in bottom right of each panel (10µm, 2µm and 1 µm in panel A, B and C respectively).

Figure 2

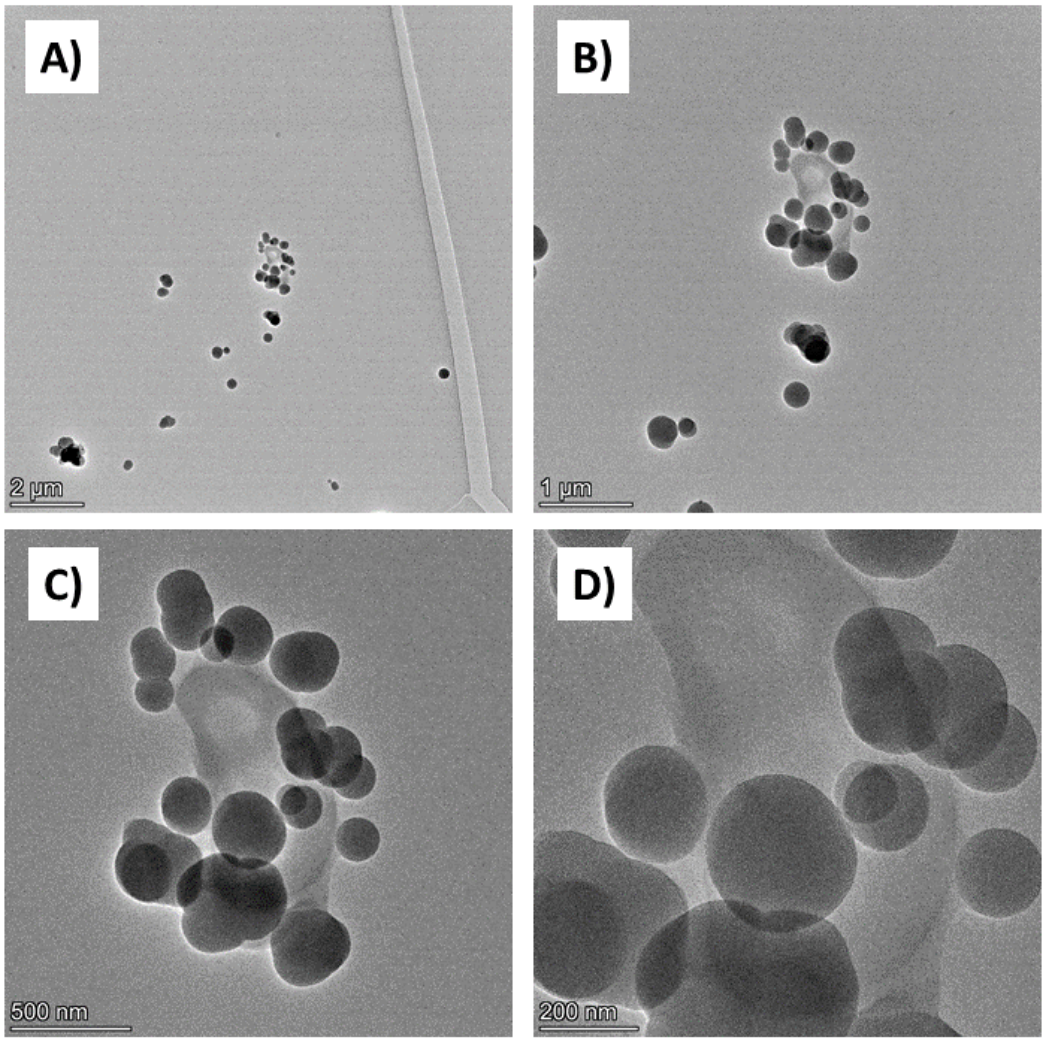

Figure 2

TEM imaging of Carbon Black. Carbon Black (AROSPERSE® 15) was imaged by with a FEI Talos F200x G2 TEM microscope at increasing resolution (A-D). Scale bar on the bottom left of each panel (2µm, 1µm, 500nm and 200nm in panel A, B, C and D respectively).

Figure 3

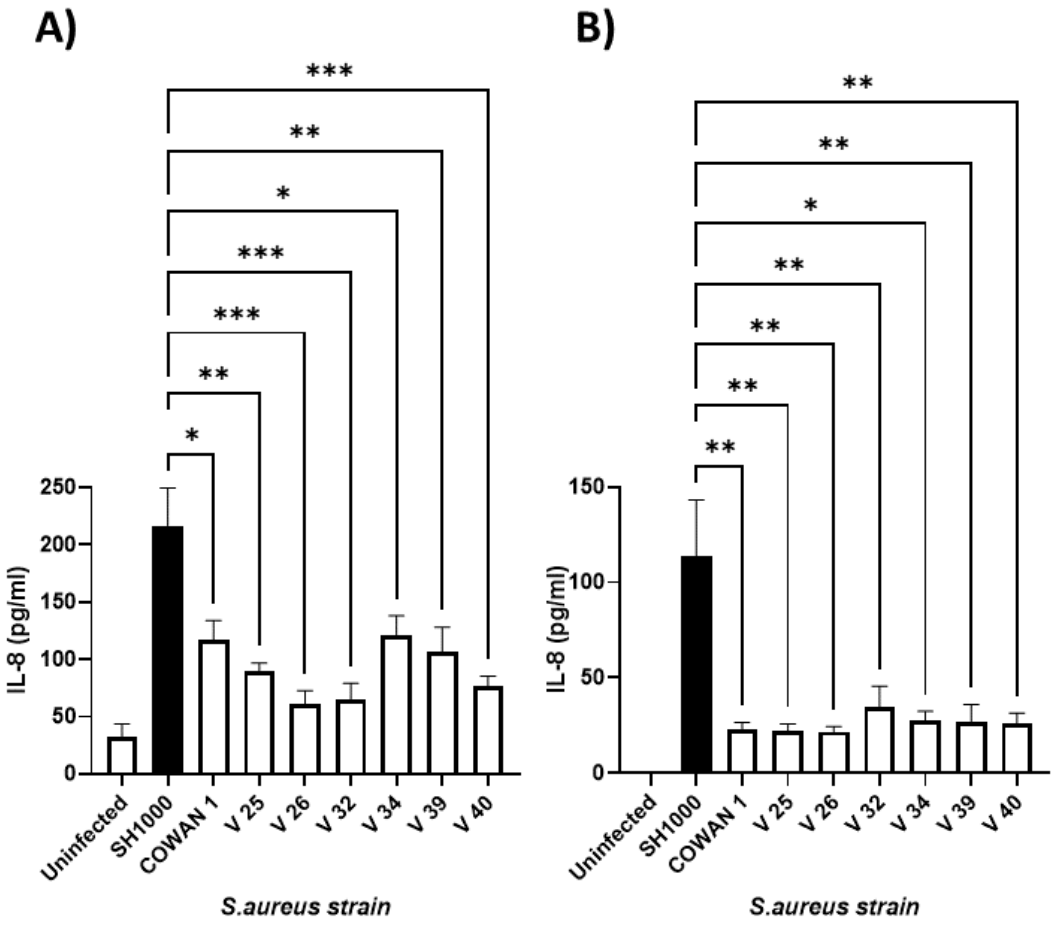

Figure 3

Selection of IL-8-inducing S. aureus strain Human HaCaT skin (A) and A549 lung (B) epithelial cells were stimulated with eight strains of S. aureus for six hours. Supernatants were collected and the concentration of IL-8 determined by ELISA. Results are expressed as the mean ± SEM of 4 experiments. Differences between treatments were calculated using an ANOVA multiple comparison test with *p<0.05,

**p<0.01, ***p<0.001 ****p<0.0001 levels considered significantly different. Black bar shows S. aureus SH1000 response.

Figure 4

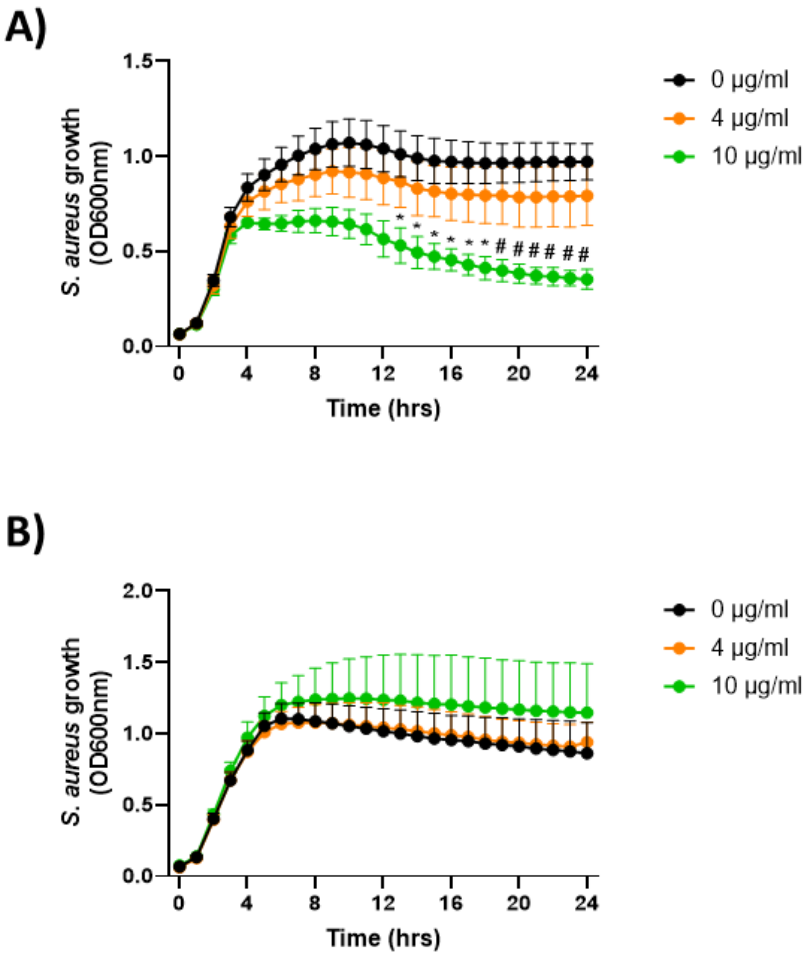

Figure 4

The effect of Carbon Black on the growth of S. aureus SH1000 One colony of S. aureus SH1000 was inoculated into 5ml of TSB and grown overnight at 37°C. Then, an equal volume of a 1:100 dilution of this preculture was added to increasing concentrations of Carbon Black (AROSPERSE® 15, (0, 4, and

10µg/ml) in (A) 1% FBS/DMEM media or (B) TSB media, and the optical density (600nm) was measured over the next 24 hours to assess growth. Results are expressed as Mean ± SEM of 3 experiments (n=3). Differences between treatments were calculated using ANOVA multiple comparison test. A *p<0.05, ##p<0.01 between 0 and 10µg/ml treatments was considered significantly different.

Figure 5

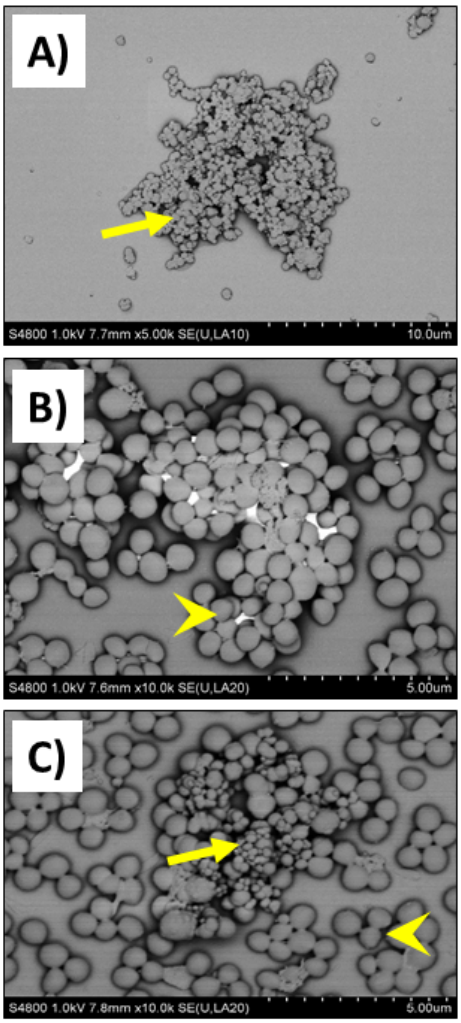

Figure 5

SEM imaging of Carbon Black and S. aureus SH1000 SEM images were generated with a Hitachi S4800 microscope to investigate Carbon Black (AROSPERSE® 15) and S. aureus interactions, aggregation and binding. A) CB (25µg/ml) alone, B) S. aureus SH1000 alone, C) CB (25µg/ml) and S. aureus SH1000. Yellow arrows show carbon black particles. Yellow arrowheads show S. aureus SH1000 bacteria. Size scale shown in bottom right of each panel.

Figure 6

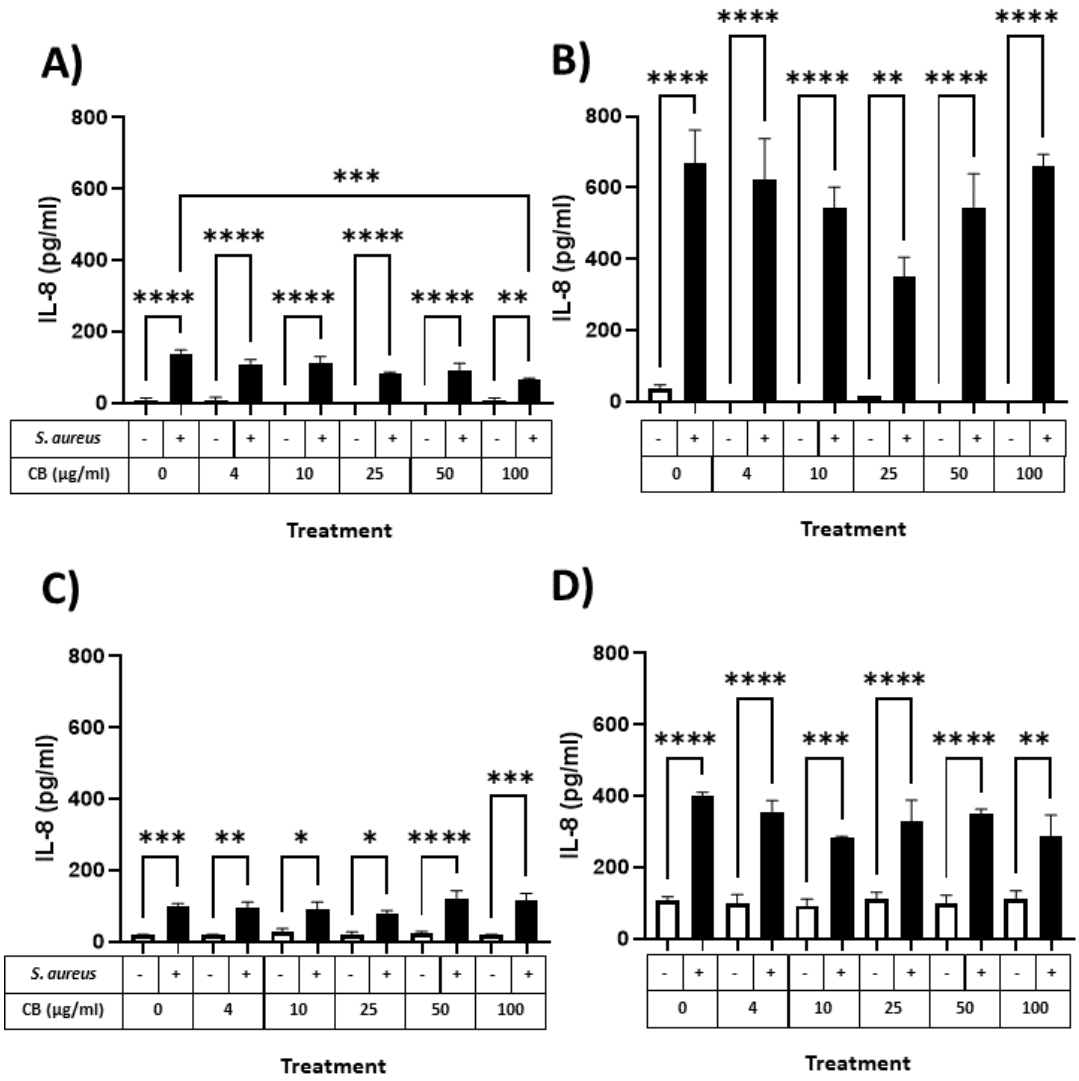

Figure 6

The effect of Carbon Black and S. aureus SH1000 on IL-8 production in epithelial cells Human HaCaT skin (A and B) and A549 lung (C and D) epithelial cells were stimulated with increasing concentrations of Carbon Black (0, 4, 10, 25, 50 and 100µg/ml) in combination with S. aureus for 5 (A and C) and 24 (B and D) hours. Supernatants were collected and the concentration of IL-8 determined by ELISA. Results are expressed as the mean ± SEM of 4 experiments. Differences between treatments were calculated using an ANOVA multiple comparison test with *p<0.05, **p<0.01, ***p<0.001 ****p<0.0001 levels considered significantly different. Black and white bars represent treatments with and without S. aureus SH1000 respectively.

Figure 7

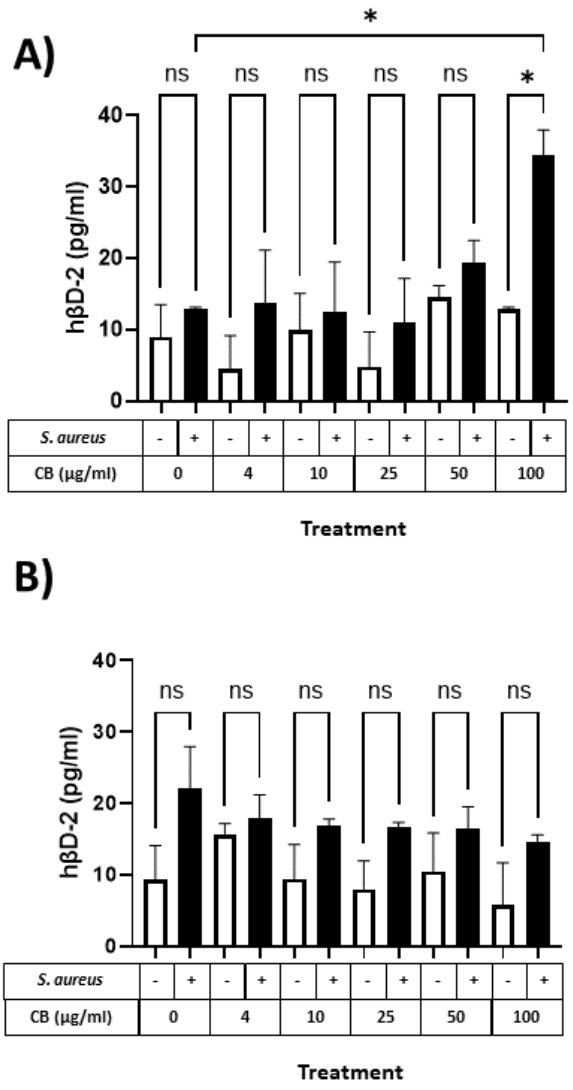

Figure 7

The effect of Carbon Black and S. aureus SH1000 on hβD-2 production in epithelial cells Human HaCaT skin (A) and A549 lung (B) epithelial cells were stimulated with increasing concentrations of Carbon Black (0, 4, 10, 25, 50 and 100µg/ml) in combination with S. aureus for 24 hours. Supernatants were collected and the concentration of hβD-2 determined by ELISA. Results are expressed as the mean ± SEM of 4 experiments. Differences between treatments were calculated using an ANOVA multiple comparison

test with *p<0.05 level considered significantly different. Black and white bars represent treatments with and without S. aureus SH1000 respectively.

Supplementary Files

This is a list of supplementary files associated with this preprint. Click to download.

- BrownSMGraphicalabstract.pptx
- Supp1.png
- Supp2.png
- Supp3.png
- Supp4.png
- Supp5.png